

# Quantum turbulence in superfluid helium: a self-consistent approach

Luca Galantucci, Andrew W. Baggaley, and Carlo F. Barenghi

*Joint Quantum Centre Durham-Newcastle, School of Mathematics,  
Statistics and Physics, Newcastle University, Newcastle upon Tyne, NE1 7RU, UK*

Giorgio Krstulovic

*Université Côte d’Azur, Observatoire de la Côte d’Azur, CNRS, Laboratoire Lagrange, Nice, France*

We study a model of superfluid dynamics at finite temperature where the superfluid component is described by the vortex filament method and the normal fluid through the Navier–Stokes equations. The dynamics of both components are fully coupled in a self-consistent manner. We study the numerical issues emerging from the coupling of the two components. The main focus of this work is the choice of the numerical scheme for distributing the mutual friction force, supported on the vortex filaments, to the mesh points where the normal fluid is defined. In particular, we show that this is a crucial aspect of the fully coupled model and a non-careful choice leads to spurious results. We propose a new scheme based on physical grounds to overcome this issue. Finally, the new numerical method to solve the fully-coupled self-consistent model is then validated numerically.

## I. INTRODUCTION

Quantum turbulence [1–3] can be loosely defined as the most general dynamical motion of tangles of quantised vortices in quantum fluids. Examples of the latter are Bose-Einstein Condensates (BECs) [4], the low temperature liquid phases of isotopes  $^3\text{He}$  and  $^4\text{He}$  and the interior of neutron stars. In the present work we will focus on the superfluid phase of  $^4\text{He}$ , frequently referred to as Helium II, which can be depicted as an intimate mixture of two fluids [5, 6]: a viscous *normal fluid* which can effectively be modelled as an ordinary (classical) Navier–Stokes fluid and an inviscid *superfluid* whose vorticity is entirely confined in one dimensional vortex lines of quantised circulation. These lines of established circulation couple the normal and superfluid components via a non-linear *mutual friction* force.

Despite the striking differences with respect to classical viscous fluids, several analogies between classical turbulence and quantum turbulence have surprisingly been established in the two last decades. For instance, experiments have revealed similar temporal decays of vorticity [7] and that He II energy spectra (which represent the distribution of kinetic energy over the length scales) obey the same classical Kolmogorov scaling at sufficiently large length scales [8–10], in agreement with theoretical [11, 12] and numerical studies [13–16]. Simultaneously, fundamental differences emerge when turbulent Helium II flows are probed at length scales smaller than the average inter-vortex spacings [17, 18] or are generated thermally as it occurs in turbulent *counterflows* [19], a regime where the superfluid and normal components move in opposite directions driven by a heat flux [20].

The comparison between quantum and classical turbulence still is a central and lively topic in low temperature physics and essential progress in the understanding of the underlying physics of quantum turbulent flows is provided by the recent development of new experimental techniques for the visualisation of superfluid helium flows. These techniques employ micron-sized tracers (both polymer particles [21] and solid hydrogen/deuterium flakes [22, 23]) and laser-induced fluorescence of metastable helium molecules [24].

Numerical simulations have also played a fundamental role in the comprehension of quantum turbulence as well as in interpreting gathered experimental data and proposing new experimental set ups. However, most numerical simulations have not investigated the fully coupled dynamics involving the normal fluid and its interplay with quantised superfluid vortices. Indeed, in many numerical studies in literature the normal fluid flow has been imposed a priori, without taking into account the back reaction Of the motion of superfluid vortices [25]. Only a minor number of investigations have addressed the fully coupled motion in A self-consistent approach. These very important efforts all present however some shortcomings: they are only confined to two-dimensional channels [26, 27]; the resolution is too limited to address fully developed turbulence in both fluid components [28]; they address simple vortex configurations [29? ]; the turbulence in the normal fluid is decaying with time (see *e.g* [31]), not reaching a statistically steady state which is of fundamental importance for the comparison of Flow statistics with the classical counterpart.

In the present research, we propose and describe a numerical algorithm aiming at tackling all these shortcomings. Our fully-coupled, three-dimensional algorithm indeed displays innovative features concerning both the numerical architecture and the physical modeling of the normal fluid - superfluid vortices interaction. Distinctive of our approach with respect to past studies is in fact the elaboration of an efficiently parallelised pseudo-spectral code capable of distributing the calculation of the normal fluid velocity field and the temporal evolution of the superfluid vortex tangle amongst distinct computational cluster nodes. This characteristic of the algorithm allows the resolution of a wider range of flow length scales compared to past studies, spanning from large, *quasi-classical* scales to small *quantum-signature* scales. This is of fundamental importance for the numerical simulation of quantum turbulent flows with parameters closer to experiments. From the physical point of view, we elaborate a local model for the mutual friction force between superfluid vortices and the normal fluid which follows the most recent creeping flow approach [32], slightly modified in order to avoid the unphysical dependence of the mutual interaction on the numerical discretisation on the vortex lines. In addition, this dissipative force between the vortices and the normal fluid (ideally a Dirac delta centred on the vortex lines) is regularised *exactly* employing the recently developed approach in classical turbulence [33, 34] for the consistent modelling of the two-way coupling between a viscous fluid and small, active particles. This approach stems from the small-scale viscous diffusion of the normal fluid disturbances generated by the vortex motion, regularising, hence, in a physically consistent manner the fluid response to vortex forcing. This is a significant improvement with respect to past algorithms which employed arbitrary numerical procedures for the distribution of the vortex forcing on the normal fluid Eulerian computational grid [35].

The paper is organised as follows. In Section II we describe the equations of motion of the superfluid, the normal fluid and the quantised vortices, with a particular emphasis on the distinct existing models for the calculation of the mutual friction force. In Section III we outline the numerical method developed, including details on the Vortex Filament Method, the Navier–Stokes solver, interpolation schemes and the procedure employed for regularising consistently the mutual friction force. Next, in Section IV, we validate our algorithm and show its application to a quantum turbulent flow. Finally, in Section V we summarize the main points addressed and outline future work.

## II. EQUATIONS OF MOTIONS

### A. Low temperature $^4\text{He}$ , a quantum fluid

At temperatures below  $T_\lambda = 2.17^\circ\text{K}$ , liquid helium undergoes a second order phase transition where its low-temperature liquid phase, known as Helium II, exhibits quantum-mechanical effects, unlike the high-temperature phase Helium I which can be adequately described as an ordinary classical newtonian fluid. In particular, according to the *two-fluid model* Helium II (frequently also referred to as He II) consists in the intimate mixture of two compenetrating fluid components [5, 6, 36–38]: a viscous *normal fluid* and an inviscid *superfluid*. Each component is characterised by its own cinematic and thermodynamic fluid variables. In this description of He II its total density  $\rho$  is the sum of the partial densities  $\rho_n$  and  $\rho_s$  (the subscripts 'n' and 's' corresponding to the normal and superfluid components, respectively), *i.e.*  $\rho = \rho_n + \rho_s$ . While  $\rho$  is approximately independent from the temperature  $T$  for  $T < T_\lambda$ , the partial densities are strongly temperature dependent: at  $T_\lambda$  He II is entirely normal;  $\rho_n/\rho$  falls very sharply with decreasing temperature, until He II is entirely superfluid in the  $T \rightarrow 0$  limit.

The normal fluid can be essentially considered an ordinary (classical) viscous Navier–Stokes fluid, with non-vanishing dynamic viscosity  $\eta$  and entropy per unit mass  $s$ . In contrast, the superfluid component is inviscid and incapable of carrying entropy and, thus, heat:  $\eta_s = s_s = 0$ . The existence of two distinct velocity fields  $\mathbf{v}_n$  and  $\mathbf{v}_s$  physically signifies that locally two simultaneous distinct movements are possible without, however, being able to distinguish the velocity field obeyed by the single particles. It is possible, therefore, to describe Helium II as a quantum fluid capable of executing *two motions at once*, each of which involves its own effective mass, even though this characteristic does not imply that Helium II can actually be separated into his distinct components.

At sufficiently low relative velocities  $v_{ns}$  between the two fluid components, the normal fluid and the superfluid are non-interacting phases, *i.e.* each component follows its own decoupled equations of motion. On the other hand, when  $v_{ns}$  exceeds a small critical value, the two fluid motions couple as a result of the nucleation in the superfluid component of a disordered tangle of thin vortex lines of quantised circulation [37, 38] (unlike classical fluids whose vorticity is a continuous field). These superfluid quantised vortex lines act in fact as scattering centers for the elementary excitations (phonons and rotons) constituting the normal fluid [39, 40] producing a momentum exchange, hence a force, between the vortex lines and the normal component.

The presence of this *mutual friction* force  $\mathbf{F}_{ns}$  in the equations of motion of both fluid components, the two fluid nature and the quantisation of circulation are all signatures of the quantum nature of Helium II. All these aspects make Helium II a richer system to investigate with respect to classical fluid dynamics. In the present study we will focus in constructing a numerical framework to address simultaneously the temporal evolution of (i) the normal fluid velocity field and (ii) the superfluid vortex tangle spatial distribution, taking into account this non-classical mutual interaction. In the following Sections II B - II E we will outline the equations of motions of the two He II fluid components and the superfluid vortex lines and the expression of the mutual friction force employed in our numerical algorithm.

### B. The normal fluid

The normal fluid can be described a gas of elementary excitations, namely phonons and rotons. In the range of temperatures which we are interested in, namely  $1.5^\circ\text{K} < T < T_\lambda$ , the normal fluid density is mostly due to rotons [40] whose mean free path is of the order of  $10^{-8}\text{m}$ , several orders of magnitude smaller than the characteristic size of current experimental facilities,  $10^{-3}\text{m} \div 10^0\text{m}$  [41, 42]. The normal component can hence be effectively described as a fluid with its own velocity  $\mathbf{v}_n$ , density  $\rho_n$ , entropy per unit mass  $s$  and dynamic viscosity  $\eta$ . Given the small temperature gradients observed in experiments [43],  $\rho_n$ ,  $s$  and  $\eta$  can be treated as uniform and constant properties of the fluid. Furthermore, the normal fluid can adequately be treated as a newtonian fluid, *i.e.* the viscous stress tensor is linear in velocity gradients. Stemming from these physical characteristics of the normal component, a long series of studies have focused on the derivation of the equations of motion of Helium II in the presence of quantised vortex lines, at lengthscales  $\Delta$  much larger than the average inter-vortex spacing  $\ell$  [40, 44–46]: these equations of motion are nowadays referred to as Hall-Vinen-Bekarevich-Khalatnikov (HVBK) equations. In the cited circumstance where the normal fluid undergoes an incompressible and isoentropic motion with constant and uniform dynamic viscosity, the HVBK equations of motion for the normal component in presence of superfluid vortices coincide with the Navier–Stokes equations for an incompressible classical viscous fluid with the addition of an extra term accounting for the

mutual friction force:

$$\rho_n \left[ \frac{\partial \mathbf{v}_n}{\partial t} + (\mathbf{v}_n \cdot \nabla) \mathbf{v}_n \right] = -\frac{\rho_n}{\rho} \nabla p - \rho_s s \nabla T + \eta \nabla^2 \mathbf{v}_n + \mathbf{F}_{ns} , \quad (1)$$

$$\nabla \cdot \mathbf{v}_n = 0 , \quad (2)$$

where  $p$  is pressure. Considering hereafter only isothermal Helium II and introducing units of length and time, respectively  $\lambda$  and  $\tau$ , Eqs. (1) and (2) can be made non-dimensional, as follows

$$\frac{\partial \tilde{\mathbf{v}}_n}{\partial \tilde{t}} + (\tilde{\mathbf{v}}_n \cdot \tilde{\nabla}) \tilde{\mathbf{v}}_n = -\tilde{\nabla} \left( \frac{\tilde{p}}{\rho} \right) + \frac{\nu_n}{(\lambda^2/\tau)} \tilde{\nabla}^2 \tilde{\mathbf{v}}_n + \left( \frac{\mathbf{F}_{ns}}{\rho_n} \right) \frac{\tau^2}{\lambda} , \quad (3)$$

$$\tilde{\nabla} \cdot \tilde{\mathbf{v}}_n = 0 , \quad (4)$$

where  $\tilde{\cdot}$  indicates non-dimensional quantities and  $\nu_n = \eta/\rho_n$  is the kinematic viscosity of the normal fluid. The numerical schemes for the integration of Eqs. (3) and (4) and the discussion concerning the open questions on the numerical handling of the mutual friction force  $\mathbf{F}_{ns}$  are illustrated in Sections III B and III D, respectively.

### C. The superfluid

The complete set of HVBK equations consists of Eqs. (1) and (2) supplemented with the equations of motion of the superfluid component which, in the incompressible approximation, are as follows:

$$\rho_s \left[ \frac{\partial \mathbf{v}_s}{\partial t} + (\mathbf{v}_s \cdot \nabla) \mathbf{v}_s \right] = -\frac{\rho_s}{\rho} \nabla p + \rho_s s \nabla T - \mathbf{F}_{ns} , \quad (5)$$

$$\nabla \cdot \mathbf{v}_s = 0 , \quad (6)$$

As already anticipated, the superfluid quantised vortex lines directly stem from the quantum nature of Helium II. More in particular, these vortex lines are topological defects of the superfluid component from which the superfluid is expelled and around which the circulation of the superfluid velocity is quantised in terms of the quantum of circulation  $\kappa = h/m$ , where  $h$  is Planck's constant and  $m$  is the mass of a  $^4\text{He}$  atom, *i.e.*

$$\Gamma = \oint_{\gamma} \mathbf{v}_s \cdot d\mathbf{l} = n\kappa \quad , \quad n \in \mathbb{Z} \quad (7)$$

The superfluid vorticity  $\boldsymbol{\omega}_s = \nabla \times \mathbf{v}_s$  is confined to these quantised vortex-lines which can effectively be described as one-dimensional objects whose core size  $a_0 \approx 10^{-10}\text{m}$  is several orders of magnitude smaller than the flow length scales probed in the present work ( $\approx 10^{-5}\text{m} \div 10^{-6}\text{m}$ ). The vortex lines can hence be treated as parametrised space curves  $\mathbf{s}(\xi, t)$  in a three-dimensional domain, where  $\xi$  is arc-length and  $t$  is time. Within this mathematical description of vortex lines, the superfluid vorticity  $\boldsymbol{\omega}_s$  can be expressed in terms of  $\delta$ -distributions, as follows

$$\boldsymbol{\omega}_s(\mathbf{x}, t) = \kappa \oint_{\mathcal{L}} \mathbf{s}'(\xi, t) \delta(\mathbf{x} - \mathbf{s}(\xi, t)) d\xi \quad , \quad (8)$$

where  $\mathbf{s}'(\xi, t) = \frac{\partial \mathbf{s}(\xi, t)}{\partial \xi}$  is the unit tangent vector to the curve  $\mathbf{s}(\xi, t)$ ,  $\mathcal{L}$  indicates the whole vortex tangle and arising from energy considerations it has been assumed that each vortex line has a single quantum of circulation ( $n$  is always equal to one in Eq. (7)).

The superfluid velocity may hence be expressed in terms of the spatial distribution of vortex lines  $\mathbf{s}(\xi, t)$  via the Biot-Savart integral [47], *i.e.*

$$\mathbf{v}_s(\mathbf{x}, t) = \nabla \phi(\mathbf{x}, t) + \frac{\kappa}{4\pi} \oint_{\mathcal{L}} \frac{\mathbf{s}'(\xi, t) \times (\mathbf{x} - \mathbf{s}(\xi, t))}{|\mathbf{x} - \mathbf{s}(\xi, t)|^3} d\xi \quad , \quad (9)$$

where  $\nabla \phi(\mathbf{x}, t)$  is the potential flow arising from the macroscopic boundary conditions. The corresponding non-dimensional equation is straightforwardly obtained and reads as follows:

$$\tilde{\mathbf{v}}_s(\tilde{\mathbf{x}}, \tilde{t}) = \tilde{\nabla} \tilde{\phi}(\tilde{\mathbf{x}}, \tilde{t}) + \frac{\kappa}{4\pi(\lambda^2/\tau)} \oint_{\mathcal{L}} \frac{\mathbf{s}'(\tilde{\xi}, \tilde{t}) \times (\tilde{\mathbf{x}} - \tilde{\mathbf{s}}(\tilde{\xi}, \tilde{t}))}{|\tilde{\mathbf{x}} - \tilde{\mathbf{s}}(\tilde{\xi}, \tilde{t})|^3} d\tilde{\xi} \quad . \quad (10)$$

The numerical computation of Eq. (10) is addressed in Section III A.

## D. The mutual friction force

Historically, in the literature two distinct theoretical frameworks have been employed to model the mutual interaction between superfluid quantised vortices and normal fluid: a *coarse-grained* philosophy and a *local* approach. The former probes the flow at length scales  $\Delta$  much larger than the average inter-vortex spacing  $\ell$  and was first derived in the pioneering studies of Hall and Vinen [39, 40] and successively employed in the studies leading to the HVBK theoretical formulation [44–46]. On the other hand, the local approach addresses Helium II dynamics at the scale of individual vortex line elements of length  $\delta < \ell$  and was first employed by Schwarz [47–49] and later reformulated by Kivotides, Barenghi and Samuels [29].

### 1. Coarse-grained mutual friction

At length scales  $\Delta \gg \ell$ , the discrete and singular nature of the superfluid vorticity field is lost. As a result, the averaged superfluid velocity and vorticity fields, indicated hereafter with  $\langle \mathbf{v}_s \rangle$  and  $\langle \boldsymbol{\omega}_s \rangle$  respectively, are *continuous* fields, smoothly varying on the macro-scale  $\Delta$ . At these scales, Hall and Vinen deduced an expression for the mutual friction force  $\langle \mathbf{F}_{ns} \rangle$  acting per unit volume on the normal fluid in a Helium II rotating bucket

$$\langle \mathbf{F}_{ns} \rangle = B \frac{\rho_n \rho_s}{2\rho \langle \boldsymbol{\omega}_s \rangle} \langle \boldsymbol{\omega}_s \rangle \times [\langle \boldsymbol{\omega}_s \rangle \times (\langle \mathbf{v}_n \rangle - \langle \mathbf{v}_s \rangle)] + B' \frac{\rho_n \rho_s}{2\rho} \langle \boldsymbol{\omega}_s \rangle \times (\langle \mathbf{v}_n \rangle - \langle \mathbf{v}_s \rangle) \quad , \quad (11)$$

where  $\langle \mathbf{v}_n \rangle$  is the coarse-grained normal fluid velocity and  $B$  and  $B'$  are mutual friction coefficients determined experimentally at scales  $\Delta$  via second sound attenuation measurements in a rotating bucket facility [39, 40]. The expression (11) has then been generalised for non-straight vortex configurations by Bekarevich and Khalatnikov [44].

### 2. Local mutual friction

In order to make progress in the understanding of Helium II turbulence and, more in particular, superfluid vortex dynamics, following the deduction of expression (11) for the mutual friction force at a macroscopic scales, Schwarz derived the expression of the force per unit length  $\langle \mathbf{f}_{sn} \rangle$  exerted by the normal fluid on a *single* vortex line element of length  $\delta < \ell$ , position  $\mathbf{s}(\xi, t)$  and unit tangent vector  $\mathbf{s}'$  [47]:

$$\langle \mathbf{f}_{sn} \rangle = -\alpha \rho_s \kappa \mathbf{s}' \times \left[ \mathbf{s}' \times \left( \hat{\mathbf{V}}_n - \mathbf{v}_s \right) \right] - \alpha' \rho_s \kappa \mathbf{s}' \times \left( \hat{\mathbf{V}}_n - \mathbf{v}_s \right) \quad , \quad (12)$$

where  $\alpha = B\rho_n/(2\rho)$ ,  $\alpha' = B'\rho_n/(2\rho)$  ( $B$  and  $B'$  being the mutual friction coefficients introduced in Eq. (11)),  $\mathbf{v}_s = \mathbf{v}_s(\mathbf{s}(\xi, t), t)$  defined by the Biot - Savart integral in Eq. (9) and  $\hat{\mathbf{V}}_n = \hat{\mathbf{V}}_n(\mathbf{s}(\xi, t), t)$  is a *prescribed* normal fluid flow.

The deduction of Eq. (12) is based on the following two important assumptions. First, it neglects the back reaction of the superfluid vortex motion on the flow of the normal fluid. It assumes in fact, that each vortex line element feels the normal fluid flow  $\langle \mathbf{v}_n \rangle$ , *i.e.* a macroscopic velocity field averaged over a region containing many vortex lines ( $\Delta \gg \ell$ ). The field  $\langle \mathbf{v}_n \rangle$  is thus determined by the macroscopic boundary conditions of the flow investigated and is entirely decoupled from the superfluid vortex tangle evolution. As a consequence, in the framework elaborated by Schwarz, the normal fluid velocity field may be prescribed *a priori*, depending on the fluid dynamic characteristics of the system studied: the explicit presence of the prescribed flow  $\hat{\mathbf{V}}_n$  in Eq. (12) aims at underlining this aspect which plays a crucial role in the present work. The second assumption, strongly linked to the previous, is the use of macroscopic coefficients  $\alpha$  and  $\alpha'$  for the calculation of the mutual friction acting on a *single* vortex element:  $\alpha$  and  $\alpha'$  are in fact simply redefinitions of the mutual friction coefficients  $B$  and  $B'$  determined at large scales  $\Delta$  in a very particular vortex line configuration (namely an lattice of straight vortex lines) [39, 40]. Equation (12) on the contrary is intended to describe the force experienced by a vortex line element in a turbulent tangle.

This decoupling of the normal fluid flow from the vortex lines motion (and, hence, the possibility of imposing arbitrarily *a priori* the normal fluid velocity field  $\hat{\mathbf{V}}_n(\mathbf{x}, t)$  felt by the vortices) confers to the theoretical framework pioneered by Schwarz a *kinematic* character: the evolution of the vortex tangle is determined for a given imposed normal flow. This local kinematic approach has been extensively employed in past studies to shed light on fundamental aspects of superfluid turbulence. In particular, various models of imposed normal flow  $\hat{\mathbf{V}}_n$  have been studied: uniform [49–52], parabolic [53–56], Hagen–Poiseuille and tail–flattened flows [57], vortex tubes [58] ABC flows [59], frozen normal fluid vortex tangles [60], random waves [52], time–frozen snapshots of turbulent solutions of Navier–Stokes

equations [52, 54, 56] and time-dependent homogeneous and isotropic turbulent solutions of linearly forced Navier–Stokes equations [61].

An alternative *dynamical* and *self-consistent* local approach has been formulated in order to take into account the back reaction of the motion of superfluid vortices onto the flow of the normal fluid [29, 30, 62]. This framework models the dragging of the roton gas of excitations constituting the normal fluid by the quantised vortices in relative motion with respect to the normal fluid itself. The velocity field hence varies at length scales smaller than the average inter-vortex spacing  $\ell$  and depends on the evolution of the vortex tangle: it cannot be prescribed, but has to be determined via the integration of the incompressible Navier–Stokes equations (1) and (2). This mismatch between the local normal fluid velocity  $\mathbf{v}_n$  perturbed by superfluid vortices (which we will hereafter refer to as *mesoscopic* normal velocity) and the macroscopic flow  $\hat{\mathbf{V}}_n$  implies the necessity of re-determining the mutual friction coefficients at these scales, now related to the local cross sections between the roton gas and the quantised vortices [62]. This self-consistent dynamical approach was first employed to investigate the normal fluid velocity field induced by simple vortex configurations, namely vortex rings [29] and vortex lines [30]. Successively, this dynamical approach has been employed to study both the forcing of the normal fluid flow by decaying superfluid vortex tangles [63, 64] and, vice-versa, the stretching of an initially small superfluid vortex tangles by either a decaying turbulent normal fluid [31, 35, 65] or decaying normal fluid coherent structures as rings [66] or Hopf links [32].

In the present work, we choose to employ the most recent formulation of the dynamical, self-consistent local approach [32], slightly revisited. Consistently with the latter, we model each superfluid vortex line element as a cylinder of radius  $a_0$  and length  $\delta$  (coinciding with the spatial discretisation of vortex lines, see Section III A for details), where  $\delta \gg a_0$ . The very small vortex core size  $a_0$  implies that when a superfluid vortex is in relative motion with respect to the normal fluid it generates a low Reynolds number normal fluid flow around the vortex itself. Typical values of the Reynolds number associated to the vortex generated normal fluid flow observed in superfluid helium experiments are  $10^{-5} \div 10^{-4}$ . Employing previous results obtained in low Reynolds number flow analysis [67–70], the force per unit length  $\mathbf{f}_D$  which the normal fluid exerts on the vortex line reads as follows

$$\mathbf{f}_D = -D \mathbf{s}' \times [\mathbf{s}' \times (\mathbf{v}_n - \dot{\mathbf{s}})] \quad , \quad (13)$$

where  $D = \frac{4\pi\rho_n\nu_n}{\frac{1}{2} - \gamma - \log\left(\frac{|\mathbf{v}_{n\perp} - \dot{\mathbf{s}}|a_0}{4\nu_n}\right)}$ ,  $\dot{\mathbf{s}} = \frac{\partial\mathbf{s}(\xi, t)}{\partial t}$  is the velocity of the vortex line (see next paragraph II E) and  $\mathbf{v}_n$  is evaluated on the vortex line element, *i.e.*  $\mathbf{v}_n = \mathbf{v}_n(\mathbf{s}(\xi, t), t)$ , the interpolation schemes being described and tested in Section III C. With  $\mathbf{v}_{n\perp}$  we indicate the component of the normal fluid velocity lying on a plane orthogonal to  $\mathbf{s}'$ . The expression (13) for the viscous force  $\mathbf{f}_D$  acting on the vortex line differs from the most recent approach [32] as it is independent of the discretisation  $\delta$  on the lines. Including further the Iordanskii force  $\mathbf{f}_I = -\rho_n\kappa \mathbf{s}' \times (\mathbf{v}_n - \dot{\mathbf{s}})$  [71, 72], the total force per unit length  $\mathbf{f}_{sn}$  acting on the superfluid vortices stemming from the interaction with the normal fluid is as follows

$$\mathbf{f}_{sn}(\mathbf{s}) = \mathbf{f}_D + \mathbf{f}_I = -D \mathbf{s}' \times [\mathbf{s}' \times (\mathbf{v}_n - \dot{\mathbf{s}})] - \rho_n\kappa \mathbf{s}' \times (\mathbf{v}_n - \dot{\mathbf{s}}) \quad . \quad (14)$$

In conclusion of this section, for the sake of completeness it is important to mention that also Eq. (12) has been employed to take into account the back reaction of the superfluid vortices on the normal fluid, by averaging  $\langle \mathbf{f}_{sn} \rangle$  on a normal fluid grid cell containing many vortex line elements [26–28].

### E. The motion of vortex lines

The equations of motion of the superfluid quantised vortex lines are of straightforward derivation once Eq. (14) is taken into account. The vortex core being very small compared to other scales of the flow implies that the vortex inertia can be neglected. As a consequence, the sum of the forces acting on a superfluid vortex has to vanish. In addition to the mutual friction force  $\mathbf{f}_{sn}$ , being the vortex in motion with respect to an inviscid fluid (the superfluid component) whose circulation around the vortex is non zero (and quantised), the vortex is subject to the Magnus force  $\mathbf{f}_M$ , which, per unit length, reads as follows

$$\mathbf{f}_M = \rho_s\kappa \mathbf{s}' \times (\dot{\mathbf{s}} - \mathbf{v}_s) \quad , \quad (15)$$

where  $\mathbf{v}_s$  is evaluated on the vortex,  $\mathbf{v}_s = \mathbf{v}_s(\mathbf{s}(\xi, t), t)$ . The equation of motion is hence  $\mathbf{f}_{sn} + \mathbf{f}_M = 0$  which, employing Eqs. (14) and (15), can be rewritten in the following form:

$$\mathbf{s}' \times [-D \mathbf{s}' \times (\mathbf{v}_n - \dot{\mathbf{s}}) - \rho_n\kappa (\mathbf{v}_n - \dot{\mathbf{s}}) + \rho_s\kappa (\dot{\mathbf{s}} - \mathbf{v}_s)] = 0 \quad . \quad (16)$$

Assuming that each vortex line element moves orthogonally to its unit tangent vector, *i.e.*  $\dot{\mathbf{s}} \cdot \mathbf{s}' = 0$ , Eq. (16) leads [32, 62] to the following equation of motion for  $\dot{\mathbf{s}}(\xi, t)$

$$\dot{\mathbf{s}} = -\mathbf{s}' \times \{\mathbf{s}' \times [(1 + \alpha) \mathbf{v}_s - \alpha \mathbf{v}_n]\} + \beta \mathbf{s}' \times (\mathbf{v}_n - \mathbf{v}_s) , \quad (17)$$

where  $\alpha = -\frac{b(1+b)+a^2}{(1+b)^2+a^2} < 0$  ,  $\beta = \frac{a}{(1+b)^2+a^2} > 0$  ,  $a = \frac{D}{\rho_s \kappa} = 4\pi \frac{\rho_n}{\rho_s} \frac{\nu_n}{\kappa} \frac{1}{\frac{1}{2} - \gamma - \log\left(\frac{|\mathbf{v}_n - \dot{\mathbf{s}}| a_0}{4\nu_n}\right)}$  and  $b = \frac{\rho_n}{\rho_s}$ . Parameter-wise, from the physical point of view the motion of the vortices is hence governed only by temperature, which determines  $\frac{\rho_n}{\rho_s}$  and  $\frac{\nu_n}{\kappa}$ .

### F. The self-consistent model

We have now introduced all the physical components to write a full self-consistent model of superfluid at finite temperature. The model comes from gathering the dimensionless equations (3), (4), (10), (14) and (17). The dimensional scaling factors  $\tau$  and  $\lambda$  can be chosen such that the integral time and length scales of the normal fluid are of order one. In particular we set

$$\nu_n^0 = \frac{\nu_n \tau}{\lambda^2}, \Gamma = \frac{\kappa}{\nu_n}. \quad (18)$$

The dimensionless viscosity  $\nu_n^0$  is set in numerics to properly resolve the small scales of the normal fluid. Note that  $\Gamma$  is dimensionless and depends on temperature. Finally, if the simulations need to be compared with experiments, physical time and length scales are recovered from Eq.(18) by choosing the unit of length of the system by setting  $\lambda$ . With this notation, the self-consistent model written in dimensionless form (after dropping tildes) reads

$$\frac{\partial \mathbf{v}_n}{\partial t} + (\mathbf{v}_n \cdot \nabla) \mathbf{v}_n = -\frac{1}{\rho_n} \nabla p + \nu_n^0 \nabla^2 \mathbf{v}_n + \frac{1}{\rho_n} \oint_{\mathcal{L}} \delta(\mathbf{x} - \mathbf{s}) \mathbf{f}_{ns}(\mathbf{s}) d\xi + \frac{1}{\rho_n} \mathbf{F}_{\text{ext}} , \quad \nabla \cdot \mathbf{v}_n = 0 \quad (19)$$

$$\mathbf{f}_{ns}(\mathbf{s}) = -\mathbf{f}_{sn}(\mathbf{s}) = -\nu_n^0 \Gamma \mathbf{s}' \times (\dot{\mathbf{s}} - \mathbf{v}_n) - \nu_n^0 D^0 \mathbf{s}' \times [\mathbf{s}' \times (\dot{\mathbf{s}} - \mathbf{v}_n)] \quad (20)$$

$$\dot{\mathbf{s}} = -\mathbf{s}' \times \{\mathbf{s}' \times [(1 + \alpha) \mathbf{v}_s(\mathbf{s}) - \alpha \mathbf{v}_n(\mathbf{s})]\} + \beta \mathbf{s}' \times (\mathbf{v}_n(\mathbf{s}) - \mathbf{v}_s(\mathbf{s})) \quad (21)$$

$$\mathbf{v}_s(\mathbf{x}, t) = \nabla \phi(\mathbf{x}, t) + \frac{\Gamma \nu_n^0}{4\pi} \oint_{\mathcal{L}} \frac{\mathbf{s}'(\xi, t) \times (\mathbf{x} - \mathbf{s}(\xi, t))}{|\mathbf{x} - \mathbf{s}(\xi, t)|^3} d\xi \quad (22)$$

with  $D^0 = \frac{4\pi}{\frac{1}{2} - \gamma - \log\left(\frac{|\mathbf{v}_n - \dot{\mathbf{s}}| a_0}{4\nu_n}\right)}$ .

In Eq.(19) we also added the external force  $\mathbf{F}_{\text{ext}}$  in order to sustain turbulence in the normal fluid. We recall that the physical parameters  $\alpha, \beta$  and  $\Gamma$  depend only on temperature. Their behaviour is displayed on Fig.1 using the tabulated values of  $\rho_n, \rho_s$  and  $\nu_n$  from reference [73].

Finally note that for a given temperature, there are two more dimensionless parameters

$$Re = \frac{v_n^{\text{rms}} L^0}{\nu_n^0} \quad \text{and} \quad I_{\text{turb}} = \frac{v_n^{\text{rms}}}{|\langle \mathbf{v}_n - \mathbf{v}_s \rangle|} , \quad (23)$$

where  $v_n^{\text{rms}}$  is the root-mean-square or the characteristic normal fluid velocity and  $L^0$  is its integral scale. The Reynolds number  $Re$  tells how turbulent is the normal fluid and turbulent intensity  $I_{\text{turb}}$  measures the strength of counterflow (or mutual friction) with respect to normal fluid turbulent fluctuations. Note that, alternatively, we can also use a Reynolds number based on the Taylor micro scale  $Re_\lambda$  of the flow, that provides a precise definition in terms of velocity gradients and fluctuations [74].

### III. NUMERICAL METHOD

The numerical integration of the self-consistent model (19 - 22) demands a special care. In particular, the coupling between the vortex filament method and the Navier-Stokes equation requires interpolations to determine the values of the normal fluid at the filament position and a redistribution of the force from  $\mathbf{f}_{ns}$  to the mesh where the normal

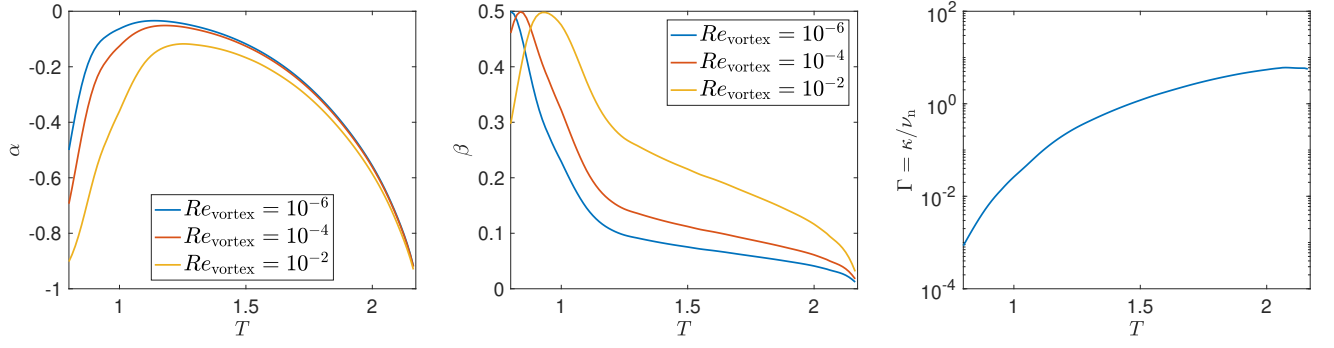


FIG. 1. Physical dimensionless parameters  $\alpha$  (left),  $\beta$  (center) and  $\Gamma$  (right) as a function of temperature. For the parameters  $\alpha$  and  $\beta$  we have used as references different vortex Reynolds numbers  $Re_{\text{vortex}} = |\mathbf{v}_{n\perp} - \dot{\mathbf{s}}|a_0/4\nu_n$ .

fluid is defined. As we will see at the end of this section, a careless treatment of the coupling immediately leads to spurious numerical artefacts.

In this section we describe the numerical method used to solve the self-consistent model (19 - 22) and we provide a physical and numerical justification for choice of the numerical scheme used for the coupling between the equations. We will first briefly described the numerical scheme of the vortex filament method and Navier–Stokes equations and later we will explain the coupling method.

### A. Vortex Filament Method

We shall briefly describe the underlying model for the motion of superfluid vortices, namely the vortex filament model (VFM). For a more in-depth overview of the model we point the reader to a recent review article [25] and references within.

The underlying assumption of the VFM is that vortices in the superfluid component can be considered one-dimensional lines, around which the circulation is quantised in terms of the quantum of circulation  $\kappa$ . Indeed, in superfluid Helium II this assumption is reasonable as the core size  $a_0$  is typically much smaller than any other characteristic length scale of the flow. There are however important phenomena, such as quantum vortex reconnections, where this assumption breaks down. We shall discuss how such events can be accounted for in the VFM at the end of present section, in paragraph III A 2.

#### 1. Vortex spatial discretisation

In order to address numerically the temporal evolution of the vortex tangle  $\mathcal{L}$ , we discretise the latter in an ordered sequence of vortex points whose time dependent position is indicated with  $\{\mathbf{s}_i(t)\}_{i=1,\dots,N_p}$ , where  $N_p$  is the number of discretisation points employed. The distance between neighbouring points is kept in the range  $[\delta/2, \delta]$  by removing or inserting additional vortex points [75]. As the vortex configuration evolves so does this Lagrangian discretisation: as the vortex length grows so does the number of discretisation points. The latter are advected by the discrete correspondent of Eq. (17), namely

$$\dot{\mathbf{s}}_i(t) = -\mathbf{s}'_i(t) \times \{\mathbf{s}'_i(t) \times [(1 + \alpha) \mathbf{v}_s(\mathbf{s}_i, t) - \alpha \mathbf{v}_n(\mathbf{s}_i, t)]\} + \beta \mathbf{s}'_i(t) \times [\mathbf{v}_n(\mathbf{s}_i, t) - \mathbf{v}_s(\mathbf{s}_i, t)] \quad , \quad (24)$$

where spatial derivatives on the vortex lines are performed employing fourth-order finite difference schemes which account for varying mesh sizes along the vortex filaments [75, 76] and time integration is performed using the third-order Adams-Bashforth method.

The dimensionless equation of motion is obtained by simply replacing velocities with their corresponding dimensionless counterpart. The interpolation of the normal fluid velocity  $\mathbf{v}_n$  on each vortex point  $\mathbf{s}_i$  presents some numerical issues, and the different tested schemes are outlined and discussed in Section III C. On the other hand, the evaluation of the superfluid velocity  $\mathbf{v}_s$  on the vortex points  $\mathbf{s}_i$  via Eq. (10), has to be dealt with caution as the Biot-Savart integral diverges for  $\mathbf{x} = \mathbf{s}_i$  when  $\mathbf{s} \rightarrow \mathbf{s}_i$ . in Eq. (10). This singularity is removed in a standard fashion by splitting the

Biot-Savart integral into a local and nonlocal contributions [48], *i.e.* (omitting time dependency to ease notation)

$$\mathbf{v}_s(\mathbf{s}_i) = \nabla\phi(\mathbf{s}_i) + \frac{\kappa}{4\pi} \log\left(\frac{\sqrt{\delta_i\delta_{i+1}}}{a_0}\right) \mathbf{s}'_i \times \mathbf{s}''_i + \frac{\kappa}{4\pi} \oint_{\mathcal{L}'} \frac{\mathbf{s}'(\xi) \times (\mathbf{s}_i - \mathbf{s}(\xi))}{|\mathbf{s}_i - \mathbf{s}(\xi)|^3} d\xi, \quad (25)$$

where  $\delta_i$  and  $\delta_{i+1}$  are the lengths of the segments  $[\mathbf{s}_{i-1}, \mathbf{s}_i]$  and  $[\mathbf{s}_i, \mathbf{s}_{i+1}]$  respectively,  $\mathbf{s}''_i = \frac{\partial^2 \mathbf{s}(\xi, t)}{\partial \xi^2} \Big|_{\mathbf{s}_i}$  is the normal vector to the curve in  $\mathbf{s}(\xi, t) = \mathbf{s}_i$  and  $\mathcal{L}'$  is the vortex tangle spatial configuration without the section between  $\mathbf{s}_{i-1}$  and  $\mathbf{s}_{i+1}$ . To match the periodic boundaries used in the integration of the Navier–Stokes equations for the normal fluid (refer to Section III B), we approximate periodicity within the VFM by periodic wrapping. This involves duplicates of the system, surrounding the computational domain with copies of itself, the contribution of these duplicate filaments being then included in the Biot-Savart integral in Eq. (25). In order to speed up the calculation of Biot Savart integrals and be able to investigate dense tangles of vortices, to compute Eq. (25) we employ a numerical method based on a tree algorithm [77] which scales as  $N_p \log N_p$  rather than  $N_p^2$ .

## 2. Quantum Vortex Reconnections

The equation (9) describing the behaviour of the superfluid velocity governed by the quantised vortex lines expresses the underlying incompressible and inviscid Euler dynamics in integral form [78]. Hence, on the basis of Helmholtz theorem, the topology of the flow ought to be frozen, *i.e.* reconnections of the quantised vortices are not envisaged. We know however from experiments [79, 80] and from more microscopic models [81–86] that superfluid vortex lines can effectively reconnect, exchanging strands with each other when they come sufficiently close, as envisaged by Feynman [87].

As a result, in order to model quantum vortex reconnections within the VFM we have to supplement Eq. (24) with an *ad-hoc* algorithmical reconnection procedure. This strategy was originally proposed by Schwarz [47], and since then a number of alternative algorithms have been proposed. Whilst this procedure is essentially arbitrary, it has been extensively tested [88] and many studies have shown good agreement between the VFM and experimental results.

## B. Navier Stokes Solver

We solve Eq.(19) by using a standard pseudo-spectral code in a three dimensional periodic domain of size  $L_x \times L_y \times L_z$ . We use  $n_x, n_y$  and  $n_z$  collocation points in each respective direction. Derivatives of the fields are directly computed in spectral space whereas non-linear terms are evaluated in physical space. The code is dealiased using the standard 2/3-rule, and therefore the maximum wavenumber is  $k_{\max} = 2\pi \min[n_x/L_x, n_y/L_y, n_z/L_z]/3$ . The main advantage of pseudo-spectral codes is that non-linear partial differential equations are solved with spectral accuracy, that means that spatial approximation errors decrease exponentially with the number of collocation points. The drawbacks are that the geometry needs to be periodic and the intense use of Fourier transforms.

The additive external forcing in Eq.(19) consists on a superposition of random Fourier modes:

$$\mathbf{F}_{\text{ext}}(\mathbf{x}) = \frac{f_0}{\mathcal{N}_f} \sum_{k_{\inf} \leq |\mathbf{k}| \leq k_{\sup}} \mathbf{F}_{\mathbf{k}} e^{i\mathbf{k} \cdot \mathbf{x}}, \quad (26)$$

with  $\mathbf{F}_{\mathbf{k}}$  a Gaussian vector of zero mean and unit variance satisfying  $\mathbf{F}_{\mathbf{k}} \cdot \mathbf{k} = 0$  (incompressibility condition) and  $\mathbf{F}_{\mathbf{k}}^* = \mathbf{F}_{-\mathbf{k}}$ .  $\mathcal{N}_f$  is a normalisation constant to impose that  $\langle |\mathbf{F}_{\text{ext}}(\mathbf{x})|^2 \rangle = f_0^2$ . A second possible choice of forcing is the so-called *frozen* forcing. It is simply obtained by setting after each time step the velocity field equal to a prescribe field for wavevectors in a predefined range. Such kind of forcing mimics a physical forcing working at constant velocity.

The pressure in the Navier–Stokes equation ensures the incompressible condition. It is easily obtained by inverting the Poisson equation

$$-\frac{1}{\rho_n} \nabla^2 p = \nabla \cdot ((\mathbf{v}_n \cdot \nabla) \mathbf{v}_n) - \frac{1}{\rho_n} \nabla \cdot \left( \oint_{\mathcal{L}} \delta(\mathbf{x} - \mathbf{s}) \mathbf{f}_{ns}(\mathbf{s}) d\xi \right). \quad (27)$$

We denote by  $\mathcal{P}$  the projector into the subspace of divergence-free functions. It is defined as  $P_{ij} = \delta_{ij} - \frac{\partial_i \partial_j}{\nabla^2}$ , with  $\partial_i = \frac{\partial}{\partial x_i}$ . The equation of motion for the normal fluid simplifies as

$$\frac{\partial \mathbf{v}_n}{\partial t} + \mathcal{P}(\mathbf{v}_n \cdot \nabla) \mathbf{v}_n = \nu_n^0 \nabla^2 \mathbf{v}_n + \frac{1}{\rho_n} \mathcal{P} \oint_{\mathcal{L}} \delta(\mathbf{x} - \mathbf{s}) \mathbf{f}_{ns}(\mathbf{s}) d\xi + \frac{1}{\rho_n} \mathbf{F}_{\text{ext}}. \quad (28)$$

In practice in numerics, we directly solve Eq.(28) as the projector  $\mathcal{P}$  takes a trivial form in Fourier space. Note that the force acting on the normal fluid due to the interaction with the filaments needs also to be projected.

Finally, remark that the mean normal fluid velocity can evolve in time due to the mutual friction force as a consequence of momentum transfer between components:

$$\frac{\partial \langle \mathbf{v}_n \rangle}{\partial t} = \frac{1}{L_x L_y L_z} \frac{1}{\rho_n} \oint_{\mathcal{C}} \mathbf{f}_{ns}(\mathbf{s}) d\xi. \quad (29)$$

### C. Interpolation Schemes

The equation of motion for the vortex filament given in (21) needs the values of the normal fluid velocity at the filament position, generically at intermesh points where the value of  $\mathbf{v}_n$  is not known. In principle, as the normal fluid is periodic, any intermesh value can be computed exactly (within spectral accuracy) by using a Fourier transform. We call this interpolation scheme *Fourier interpolation* and it will be used as benchmark for comparisons. The Fourier interpolation is extremely costly and prohibitive for practical applications, as it requires  $n_x n_y n_z$  evaluations of complex exponentials per point of a vortex filament. Affordable interpolation schemes are typically defined on physical space and their accuracy depends on order of the method and on the regularity of the fields. The most commonly used schemes in three dimensions are *Nearest neighbours*, where the value of closest grid point is taken and *Tri-Linear* and *Tri-Cubic*, where the interpolation is performed in each direction by a line or a cubic polynomial. More recently, a new approach based on fourth-order *B-splines* has been proved to be specially well adapted to pseudo-spectral codes, non expensive and highly accurate [89].

In order to study the effect of different interpolation schemes, we study how a vortex ring moves in a static spatially dependent flow. We do not take into account yet the retroaction of the vortex filament on the normal fluid. We consider a domain of size  $L_x = L_y = L_z = 2\pi$  and a normal fluid being a superposition of ABC flows at different scales. The normal fluid is defined as follows:

$$\mathbf{v}_n(x, y, z) = \sum_{n=1}^{n_{\max}} (B \cos ny + C \sin nz, A \sin x + C \cos nz, A \cos nx + B \sin ny), \quad (30)$$

with  $A = 1, B = -1, C = 5$  and  $n_{\max} = 10$ . We evaluate the field in a mesh with  $N = 128$  and 256 collocation points in each direction. As the largest wavevector is  $\sqrt{3}n_{\max}$ , the Fourier interpolation is exact (up to round noise errors).

We initialise a vortex ring of size  $R = 0.2387$  and set the temperature at  $T = 1.95^\circ\text{K}$ . We let the ring evolve with the static normal fluid in the background. As the ring evolves it deforms because of the highly non-homogenous normal fluid. In order to obtain a quantitative comparison between different schemes, we measure the mean radius of the ring as a function of time  $R(t) = \langle |\mathbf{s}(\xi) - \mathbf{s}_{\text{center}}| \rangle$  where  $\mathbf{s}_{\text{center}} = \langle \mathbf{s} \rangle$  and the average is performed over vortex points. The temporal evolution of  $R(t)$  is displayed in Fig.2 for two different resolutions and different interpolation schemes. As expected, it is apparent that the error decreases when the number of collocation points of the normal

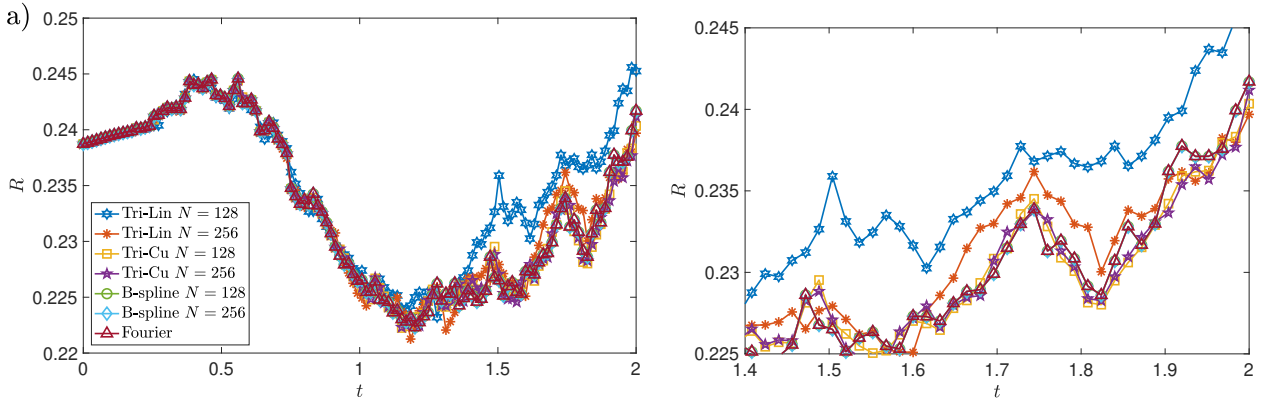


FIG. 2. (Color online) Temporal evolution of the mean radius of a ring for different interpolation schemes and normal fluid grid resolutions (arbitrary units). The right figure displays a zoom at later times.

fluid grid increases. It is also clear, that Tri-linear interpolation gives very poor results.

To better quantify the accuracy of the interpolation methods, we compute the relative error of the radius respect to the reference one obtained by Fourier interpolation  $|R(t) - R_{\text{ref}}(t)|/R_{\text{ref}}(t)$ . Its time evolution is displayed in Fig.3.

Remarkably, the B-spline interpolation is found to reduce considerably the interpolating errors. The extra cost of this

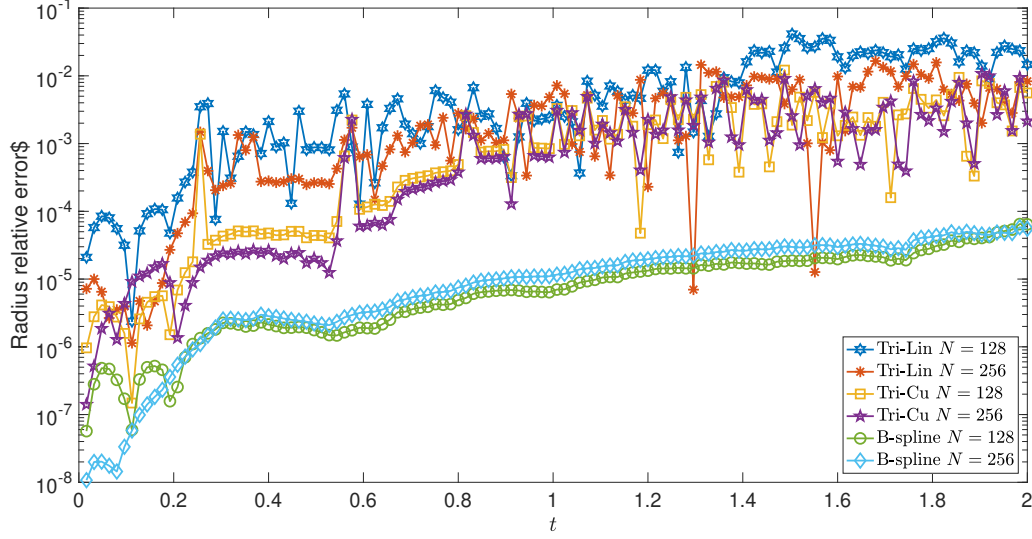


FIG. 3. (Color online). Temporal evolution of the relative error  $|R(t) - R_{\text{ref}}(t)|/R_{\text{ref}}(t)$ , where the reference evolution is obtained with Fourier interpolation (arbitrary units).

scheme is just one single fast Fourier transform independently the number of points to be interpolated. We chose this interpolation method to numerical integrate the self-consistent model.

#### D. Mutual Friction Force distribution

We now discuss the retro-action of the motion of vortex filaments on the equation for the normal fluid. This force, seen from the normal fluid, is  $\delta$ -supported on the vortex-lines identified by the  $N_p$  vortex points  $\{\mathbf{s}_i(t)\}_{i=1,\dots,N_p}$  and thus needs to be distributed on the grid points where the normal fluid is computed. More precisely, we denote by  $(\alpha, \beta, \gamma)$ , with  $\alpha, \beta, \gamma \in [0, 1]$ , the neighboring grid points of  $\mathbf{s}_i(t)$ . The force  $\mathbf{f}_{\text{ns}}(\mathbf{s}_i(t))$  exerted by the vortex filament on the normal fluid has to be distributed among neighbouring points using some weights  $w_{\alpha,\beta,\gamma}$ , as displayed in the sketch of Fig.4.

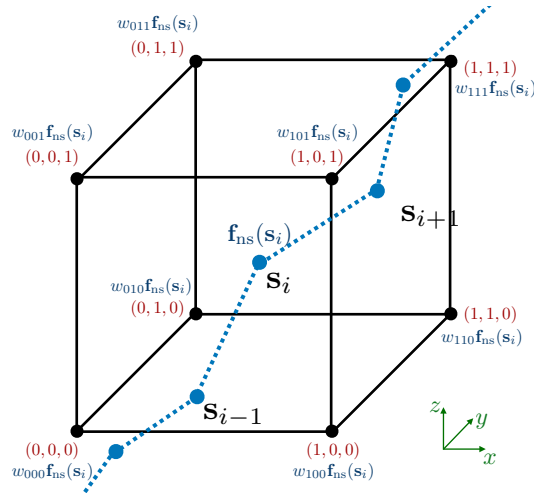


FIG. 4. Sketch of the force distribution and weights.

By definition, the weights satisfy  $\sum_{\alpha,\beta,\gamma=0}^1 w_{\alpha\beta\gamma} = 1$ . After distribution of the force, some smoothing of the resulting force field could be in principle performed. This kind of numerical problem is often faced in active matter systems, where small point-like particles (*i.e.* swimmers, plankton, bacteria) retro-act on a classical turbulent flow. Let's rewrite the the normal fluid equation considering the discretisation of the vortex lines discussed in Section III A:

$$\frac{\partial \mathbf{v}_n}{\partial t} + \mathcal{P}(\mathbf{v}_n \cdot \nabla) \mathbf{v}_n = \nu_n^0 \nabla^2 \mathbf{v}_n + \frac{1}{\rho_n} \sum_{i=1}^{N_p} \mathcal{P} \delta(\mathbf{x} - \mathbf{s}_i(t)) \mathbf{f}_{ns}^i(t) \delta_i, \quad (31)$$

where  $\mathbf{f}_{ns}^i(t) := \mathbf{f}_{ns}(\mathbf{s}_i(t))$ ,  $\delta_i$  is the length of the  $i$ -th vortex line element and the dependence on time of the mutual friction force has been explicitly reported as it will be play an important role in the subsequent part of the discussion. For the sake of simplicity, the external force has been omitted in Eq. (31) and a simple Riemann sum has been used to approximate the line integral. Note that a trapezoidal rule, which is a better approximation, may be numerically used by simply replacing  $\delta_i \rightarrow (\delta_i + \delta_{i+1})/2$  and readjusting the indices of the sum. It is thus evident that our problem is formally identical to coupling discrete, point-like, active particles to the turbulent flow of a classical viscous fluid.

It is well known that in systems dealing with active matter relevant physical quantities (*e.g.* aggregation and condensation, mixing, growing of species, etc.) may strongly depend on the choice of the force distribution method and the filtering scale [33, 34]. The same kind of unphysical issues appear in our self-consistent model. In order to illustrate this problem, we consider the simple case of a vortex ring moving in a initially quiescent normal fluid, similar to the setting studied in [29]. We consider a ring of radius  $R = 0.2387$  and set the temperature at  $T = 1.95^\circ\text{K}$ . Because of mutual friction, the ring is expected to shrink. We compare the temporal evolution of its radius employing different filtering methods. We distribute the force to the nearest neighbour grid points, *i.e.*  $w_{\alpha,\beta,\gamma} = 0$  for all grid points except the nearest one to  $\mathbf{s}_i$ . The resulting force field is then filtered by using either a moving average over  $N_{\text{filter}}$  points or a Gaussian kernel of width  $N_{\text{filter}} \Delta x$ , where  $\Delta x = L_x/N_x$  is the mesh size. Figure 5 displays the temporal evolution of the vortex ring radius for the different schemes. It is clear that dynamics of the ring and its shrinking rate is strongly dependent on the employed filtering procedure. Such dependence is clearly spurious and

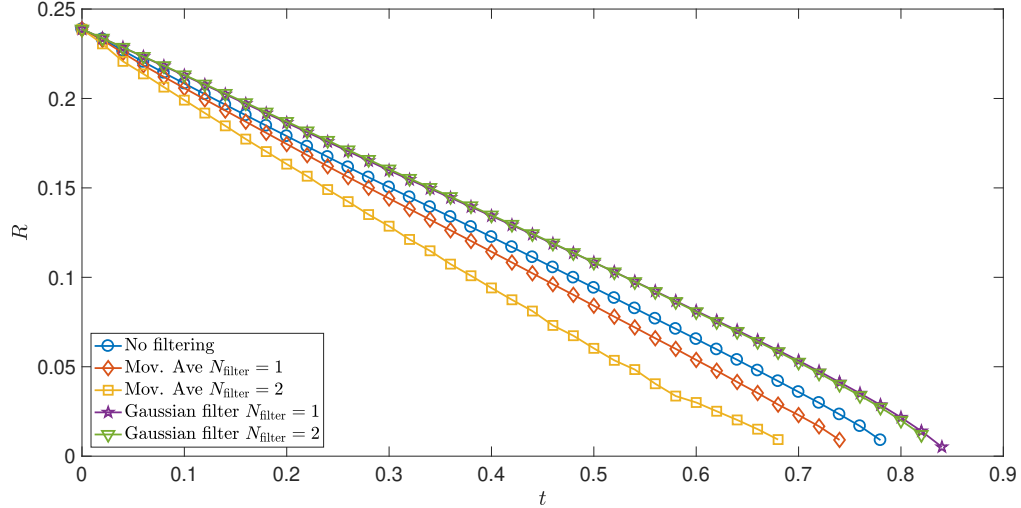


FIG. 5. (Color online). Temporal evolution of the radius of a vortex ring with in an initially constant a quiescent normal fluid. The force acting on the normal fluid is distributed to the nearest neighbour point of the mesh. Different filtering procedures are tested.

there is an evident necessity for a numerical method based on a physical background. In order to achieve this aim, we adopt the recently developed, rigorous regularisation approach capable of taking into account the strongly localised, singular response of point-like particles in classical turbulence [33, 34]. The advantage of this framework is that the regularization of the momentum coupling between point-like particles and viscous flows is based on the physics of vorticity generation and its viscous diffusion at very small scales: the two-way coupling is addressed in a physical consistent manner. Essential for our objective is that this regularisation may be employed in our quantum turbulent context as the Reynolds number of the flow (based on the atomic size of the quantised vortex core, the normal fluid - superfluid vortex relative velocity and the normal fluid viscosity) is very small.

In brief (we refer the reader to the original papers [33, 34] for further details), the approach we borrow from classical turbulence is based on the solution of the delta-forced linear unsteady Stokes equation. Accordingly to the classical formulation, we introduce the time-delay  $\epsilon_R$  coinciding with the time interval during which the singular, localised, instantaneously generated vorticity arising from the relative vortex motion with respect to the normal fluid is diffused to the relevant hydrodynamic scales of the flow, *i.e.* the spacing  $\Delta x$  of the computational grid which the normal fluid velocity field is calculated on. This finite time delay  $\epsilon_R$  naturally regularises the delta-shaped nature of the mutual friction force  $\mathbf{f}_{ns}^i(t)\delta(\mathbf{x} - \mathbf{s}_i(t))$  via the fundamental solution of the diffusion equation

$$g[\mathbf{x} - \mathbf{s}_i(t - \epsilon_R), \epsilon_R] = \frac{1}{(4\pi\nu\epsilon_R)^{3/2}} \exp\left[-\frac{\|\mathbf{x} - \mathbf{s}_i(t - \epsilon_R)\|^2}{4\nu\epsilon_R}\right], \quad (32)$$

a Gaussian with standard deviation  $\sigma_R = \sqrt{2\nu\epsilon_R}$ . The resulting expression for the mutual friction force exerted by the  $i$ -th vortex line element on the normal fluid at generic time  $t$  in a point  $\mathbf{x}$  is  $\mathbf{f}_{ns}^i(t - \epsilon_R)g[\mathbf{x} - \mathbf{s}_i(t - \epsilon_R), \epsilon_R]\delta_i$  [33, 34] yielding the following modified Navier–Stokes equation for the normal fluid velocity field:

$$\frac{\partial \mathbf{v}_n}{\partial t} + \mathcal{P}(\mathbf{v}_n \cdot \nabla) \mathbf{v}_n = \nu_n^0 \nabla^2 \mathbf{v}_n + \frac{1}{\rho_n} \sum_{i=1}^{N_p} \mathcal{P} \mathbf{f}_{ns}^i(t - \epsilon_R) g[\mathbf{x} - \mathbf{s}_i(t - \epsilon_R), \epsilon_R] \delta_i. \quad (33)$$

From the physical point of view, Eq. (33) implies that the strongly localised vorticity injected in the normal flow by the relative motion of the vortices is neglected until it has been diffused by viscosity to a characteristic length scale  $\sigma_R = \sqrt{2\nu\epsilon_R}$ . To be consistent and in order to take into account the vortex induced disturbances as soon as the relevant hydrodynamic scales are affected, we choose the finite time delay  $\epsilon_R$  so that  $\sigma_R/\Delta x = 1$ . The extensive tests performed in the original paper [33] ensure that  $\sigma_R/\Delta x = 1$  is a suitable choice.

In theory, for each  $i$ -th vortex line element it is possible to compute the corresponding weight for each point of the numerical grid: it would sufficient to integrate the Gaussian kernel  $g[\mathbf{x} - \mathbf{s}_i(t - \epsilon_R), \epsilon_R]$  over the volume  $\Delta V = \Delta x \Delta y \Delta z$  centred on the grid point. For instance, as displayed in the two-dimensional sketch of Fig.6, the force coming from the  $i$ -th vortex element at  $\mathbf{s}_i$  contributes to the force computed on mesh point  $\mathbf{x}$ , but also on mesh point  $\mathbf{z}$ , the weights being the integral of  $g(\mathbf{x} - \mathbf{s}_i, \epsilon_R)$  over their respective cells, represented by dashed squares in the sketch. This procedure would have to be repeated on each grid point for each vortex element: although exact, this approach is extremely costly. In addition, always referring to Fig.6, the weight corresponding to mesh point  $\mathbf{z}$  is very small as we choose  $\sigma_R/\Delta x = 1$ ; the diffusion based regularisation which we employ localises in fact the force in a sphere of radius  $\sigma_R$  centred at  $\mathbf{s}_i$ . As a consequence, instead of distributing the force on each grid point by computing  $N_x N_y N_z N_p$  integrals  $g(\mathbf{x} - \mathbf{s}_i, \epsilon_R)$  all over the grid, we distribute the force only to neighbouring mesh points of  $\mathbf{s}_i$ , taking care of including the weights of far grid points. Proceeding in this fashion, the total force is preserved, as the integral of  $\int_{\mathbb{R}^3} g[\mathbf{x} - \mathbf{s}_i(t - \epsilon_R), \epsilon_R] d\mathbf{x} = 1$ . As matter of example, in the sketch outlined in Fig.6, the  $\mathbf{f}_{ns}(\mathbf{s}_i)$  of point  $\mathbf{s}_i$  will be distributed among only the four neighbouring points. In order to use a conservative scheme, for each of the neighbouring points the Gaussian kernel  $g(\mathbf{x} - \mathbf{s}_i, \epsilon_R)$  will be integrated on the corresponding full quadrant (octant in three dimensions): in the two-dimensional simplified sketch in Fig.6, this corresponds to integrating  $g$  over the region coloured in green for point  $\mathbf{x}$  and over the yellow region for point  $\mathbf{y}$ . The generalisation to three dimension is straightforward. The advantage of this approach is that the space integrals of  $g$  may actually be computed analytically.

The computations of the integrals leads to weights  $w_{\alpha\beta\gamma}$  that will be used to distribute the force among the neighbouring grid points of  $\mathbf{s}_i$ , corresponding to sketch and notation of Fig.4. Note that because the Gaussian kernel

$g$  is normalised to one, we have by construction that  $\sum_{\alpha,\beta,\gamma=0}^1 w_{\alpha\beta\gamma} = 1$ . To compute the weights  $w_{\alpha\beta\gamma}$ , we first note

that the integrals of  $g(\mathbf{x} - \mathbf{s}_i, \epsilon_R)$  can be factorised in each cartesian direction: we will therefore only compute the contribution in the  $x$  direction, the computation of the contributions of the other directions is formally identical. The weight for the grid point of the left of  $s_i^x$  (indicated with  $\lfloor s_i^x \rfloor$ , corresponding to  $\alpha = 0$ ) results from the one-dimensional integral over  $(-\infty, \lfloor s_i^x \rfloor + \frac{\Delta x}{2})$ , whereas the weight for the grid point on the right ( $\lfloor s_i^x \rfloor + \Delta x$ ,  $\alpha = 1$ ), stems from the integral over  $(\lfloor s_i^x \rfloor + \frac{\Delta x}{2}, \infty)$ . The one-dimensional weight is hence straightforwardly computed and reads as follows

$$w_\alpha[s_i^x] = \alpha + (1 - 2\alpha) \frac{1}{2} \left( 1 + \text{Erf} \left[ -\frac{\tilde{s}_i^x - \frac{1}{2}}{\sqrt{2}(\sigma_R/\Delta x)} \right] \right) \quad (34)$$

$$\tilde{s}_i^x = \frac{s_i^x - \lfloor s_i^x \rfloor}{\Delta x} \in [0, 1]. \quad (35)$$

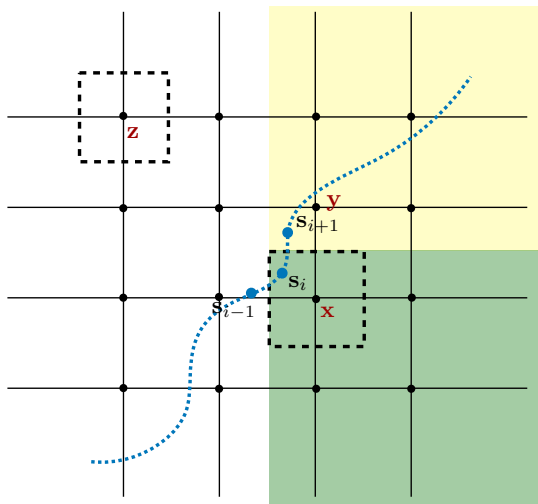


FIG. 6. (Color online). Two-dimensional sketch of the force distribution method.

The integrals  $w_\beta[s_i^y]$  and  $w_\gamma[s_i^z]$  over the two remaining directions are performed in the same fashion. The diffusion-based weights for the three dimensional grid are finally given by

$$w_{\alpha\beta\gamma} = w_\alpha[s_i^x]w_\beta[s_i^y]w_\gamma[s_i^z] \quad (36)$$

### E. Numerical Strategy and Parallelisation

The numerical integration of the fully-coupled self-consistent model has been implemented taking advantage of modern parallel computing. The solvers of the vortex filament method and the Navier–Stokes equations are of very different nature and they only need to interact through the evaluation of the mutual friction force. In this first version of the solver, we have opted for an hybrid OpenMP-MPI parallelisation scheme. Both, the vortex filament and Navier–Stokes solvers are handled by different MPI processes. Each MPI process contains many OpenMP threads, so each solver is also independently parallelised by using this shared memory library. The evaluation of the mutual friction force requires the communication between the two solvers that do not have access to each other fields and variables. The communication is managed through the Message Passing Interface (MPI) library at the end of each time step and the mutual friction is then applied. This kind of scheme is naturally adapted to modern clusters that contain many nodes, with each node having a large number of cpus having shared memory.

Finally, the values of the time steps for the Navier–Stokes equations and the vortex filament solver might be very different, being the vortex filament typically smaller. In order to speed up the code, depending on the physical problem, each solver can perform sub-loops (in time) to ensure numerical stability and an efficient integration of the full model.

## IV. EXAMPLES

In this short section we show two physical applications of the full self-consistent model. We do not intend to introduce any new physical phenomena in this section, we want to validate our approach and show the computational capabilities of our implementation.

We first study the configuration investigated in the pioneer work of Kivotides et al. [29], namely a vortex ring moving in a initially quiescent normal fluid. In that work, it was observed that due to the interaction between the two components, two normal fluid vortex rings are created accompanying the superfluid vortex ring. We integrate our self-consistent model using as initial condition a vortex ring of radius  $R = 0.2387$  in a box of size  $2\pi$  and set the temperature to  $T = 1.95^\circ\text{K}$ . A visualisation of the simulation is displayed in Fig.7. The superfluid vortex ring is displayed in green whereas the two resulting normal fluid vortex rings are rendered in reddish colours. We also show a slice perpendicular to vortex ring, where the normal velocity component in the direction of the movement of the vortex rings is rendered in blue colours. A wake behind the rings is apparent.

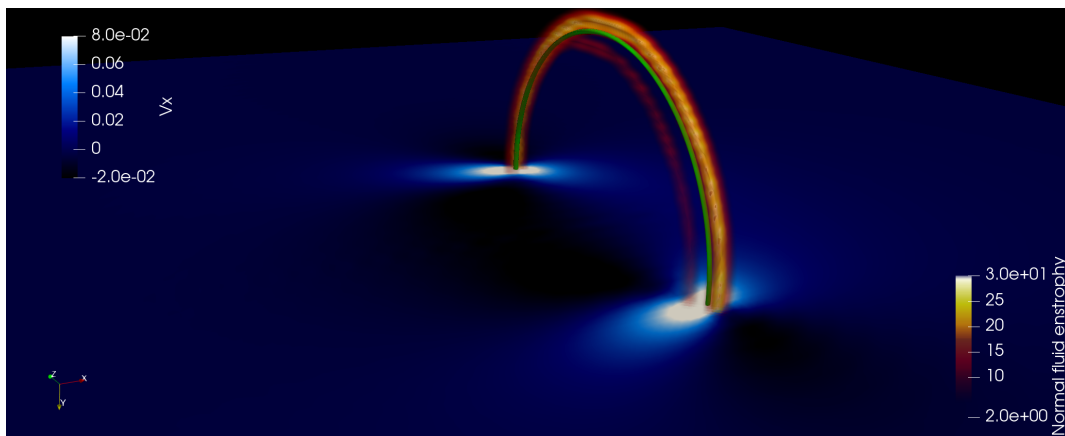


FIG. 7. (Color online). Evolution of a superfluid vortex ring in normal fluid initially at rest. The normal fluid enstrophy is displayed by the yellow-orange-black rendering whereas the superfluid vortex ring corresponds to the green line. The normal fluid velocity component in the direction of the movement of the ring is also rendered in blue on a slice perpendicular to the vortices.

Our implementation of the self-consistent model naturally allows us to study the effect of normal fluid turbulence in the dynamics of vortex rings. As discussed in section III B, we can easily add an external forcing  $\mathbf{F}_{\text{ext}}$  to the Navier–Stokes equations in order to sustain turbulence. We first produce a turbulent state using a volumetric external forcing, where  $\mathbf{F}_{\text{ext}}$  is equal to the ABC flow defined in Eq.(30), but only on the largest scales ( $n_{\text{max}} = 1$ ). We use a resolution of  $256^3$  points, which allows us to obtain a Reynolds number based on the Taylor micro-scale  $Re_\lambda = 127$ . Once, the turbulent state is prepared, we study the evolution of a ring of radius  $R = 0.2387$  in a box of size  $2\pi$  at temperature  $T = 1.95^\circ\text{K}$ . The initial condition used in our self-consistent method is displayed in Fig.8 (top left panel). We clearly observe the turbulent fluctuations of the normal fluid displayed by the reddish rendering of the normal fluid enstrophy. As the time evolves, the turbulent fluctuations destabilise the ring, inducing large amplitude Kelvin waves. After a couple of large-eddy-turnover times, the vortex filament will self-reconnect leading to more and more complex rings that will finally create a turbulent superfluid vortex tangle in equilibrium with the turbulent normal fluid.

It is apparent from the visualisations of the temporal evolution of the ring that normal fluid fluctuations are responsible for an increase of the total vortex length. In Fig.9 we display the temporal dependence of the total vortex length. Remarkably, there is a change on the behaviour at times of the order of one  $T_L$ , indicating that normal fluid fluctuations should play an important role in quantum turbulence. This is an interesting question with important consequences on current quantum turbulent experiments. It is also natural to expect that the evolution of the vortex length might strongly depend on temperature and on the initial superfluid vortex configuration. It is clear that, a performant, accurate and physically sound solver of the fully-coupled self-consistent model of quantum turbulence will lead to a very novel research on turbulent quantum fluids.

## V. CONCLUSIONS

In this investigation we have outlined a novel algorithm for the numerical simulation of quantum turbulence at finite temperatures. Distinctive of our numerical architecture are (i) the parallelised, efficient, pseudo-spectral code, capable of distributing the calculation amongst distinct computational cluster codes, and (ii) the forcing scheme employed for the normal fluid. These features allow to resolve a wider range of flow length scales compared to previous studies, spanning from large, quasi-classical scales to small, quantum peculiar ones. This is of fundamental importance in order to address and investigate the characteristics of quantum turbulence shared with the classical counterpart, and the features specific to quantum turbulent flows.

From the physical modelling point of view, we introduce a novel, local approach to the computation of the mutual friction force, stemming from creeping flow analysis and independent of the numerical discretisation on the vortex lines. In addition, we have also implemented an exact regularisation of the mutual friction force based on the small-scale viscous diffusion of the disturbances generated by vortex motion in the normal fluid. Overall, the numerical algorithm contains thus significant innovations with respect to numerical codes previously described in literature.

After a detailed description of all the distinct features of our algorithm, we validate the latter by calculating the normal fluid structures generated by the motion of a quantum vortex ring, recovering the “triple vortex ring” observed

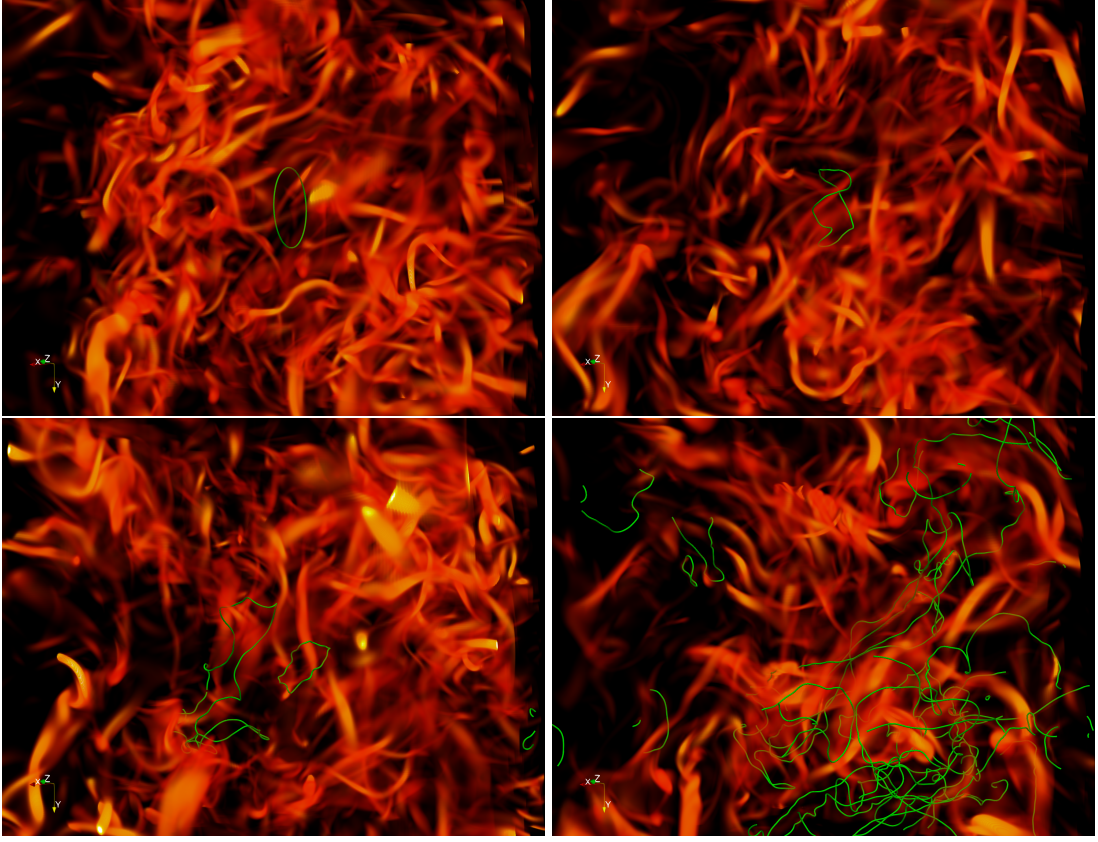


FIG. 8. (Colour online). Evolution of a superfluid vortex ring in turbulent normal fluid. The norm fluid enstrophy is displayed by the yellow-orange-black rendering whereas the superfluid vortex ring corresponds to the green line. The corresponding times are  $t = 0$ ,  $t = 0.5T_L$ ,  $t = 2.8T_L$  and  $t = 5.5T_L$ , where  $T_L$  is the large eddy-turnover time of the normal fluid.

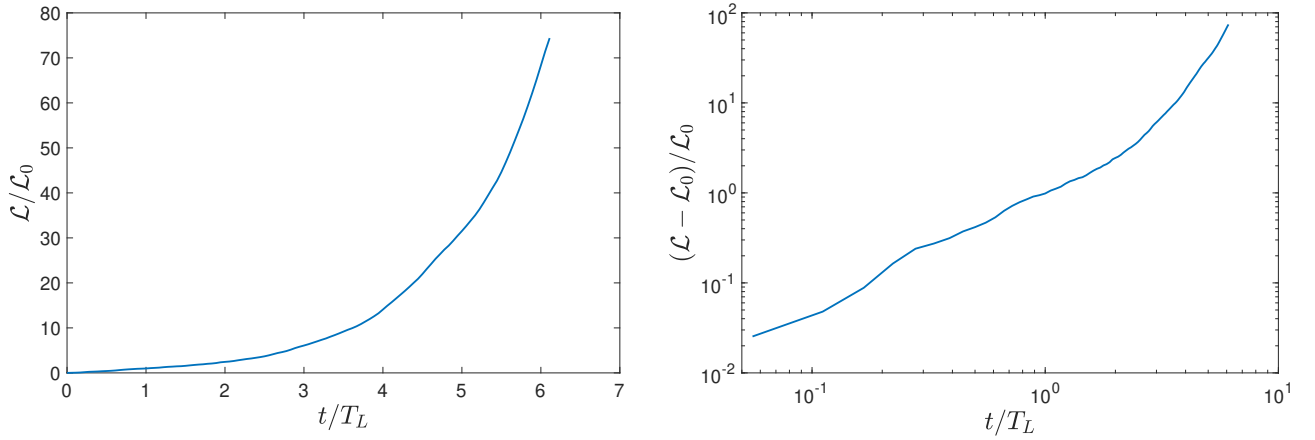


FIG. 9. (Color online). Temporal evolution of the total vortex length  $\mathcal{L}$  resulting from a (initially perfect) vortex ring of length  $\mathcal{L}_0 = 2\pi R$  in a turbulent normal fluid background.  $\mathcal{L}$

in the pioneering work performed at the beginning of the century [29]. Subsequently, we show the capability of our numerical code to simulate the temporal evolution of a superfluid vortex tangle, resolving a wider range of flow length scales compared to state of the art numerical simulations.

In conclusion, our novel algorithm paves the way for a new series of investigations of quantum turbulence at finite

temperatures. For instance, the wider range of scales resolved by the algorithm, thanks to the high parallelisation of the code, and the numerical scheme employed for the forcing of the normal fluid, open the possibility of investigating numerically the statistically steady-state characteristics of the velocity fields of the normal and superfluid components at scales smaller than the average inter-vortex spacing, where the singular and quantised nature of the vortices is expected to play a fundamental role. The insight gained could prove to be very important for *e.g.* the comprehension of the microscopic mechanisms leading to the locking of the energy spectra of the normal fluid and the superfluid component, when turbulence is forced mechanically. Finally, the extension of the numerical algorithm described in the present study to thermal counterflow turbulence could allow to better characterise this turbulent regime which does not have a classical analogue and occurs without an energy cascade [20].

- 
- [1] WF Vinen and JJ Niemela. Quantum turbulence. *J Low Temp Phys*, 128:167, 2002.
  - [2] L Skrbek and KR Sreenivasan. Developed quantum turbulence and its decay. *Phys Fluids*, 24:011301, 2012.
  - [3] CF Barenghi, L Skrbek, and KP Sreenivasan. Introduction to quantum turbulence. *Proc Natl Acad Sci USA*, 111(1):supp 1, 4647, 2014.
  - [4] L. P. Pitaevskii and S. Stringari. *Bose-Einstein condensation*. Ox Univ Pr, 2003.
  - [5] L. Tisza. Transport phenomena in helium ii. *Nature*, 141:913, 1938.
  - [6] L.D. Landau. Theory of the superfluidity of helium ii. *J. Phys U.S.S.R.*, 5:71, 1941.
  - [7] S. R. Stalp, L. Skrbek, and R. J. Donnelly. *Phys Rev Lett*, 82:4831, 1999.
  - [8] J Maurer and P Tabeling. Local investigation of superfluid turbulence. *Europhys Lett*, 43:29, 1998.
  - [9] J. Salort, C. Baudet, B. Castaing, B. Chabaud, F. Daviaud, T. Didelot, P. Diribarne, B. Dubrulle, Y. Gagne, F. Gauthier, A. Girard, B. Henbral, B. Rousset, P. Thibault, and P. E. Roche. Turbulent velocity spectra in superfluid flows. *Phys Fluids*, 22:125102, 2010.
  - [10] CF Barenghi, V L'vov, and PE Roche. Experimental, numerical and analytical velocity spectra in turbulent quantum fluid. *Proc Natl Acad Sci USA*, 111(1):supp 1, 4683, 2014.
  - [11] VS L'vov, S Nazarenko, and L Skrbek. Energy spectra of developed turbulence in helium superfluids. *J Low Temp Phys*, 145:125, 2006.
  - [12] VS L'vov, S Nazarenko, and O Rudenko. Gradual eddy-wave crossover in superfluid turbulence. *J Low Temp Phys*, 153:150, 2008.
  - [13] AW Baggaley, J Laurie, and CF Barenghi. Vortex-density fluctuations, energy spectra, and vortical regions in superfluid turbulence. *Phys Rev Lett*, 109:205304, 2012.
  - [14] A. W. Baggaley and C. F. Barenghi. Vortex-density fluctuations in quantum turbulence. *Phys Rev B*, 84:020504, 2011.
  - [15] T Araki, M Tsubota, and SK Nemirovskii. Energy spectrum of superfluid turbulence with no normal-fluid component. *Phys Rev Lett*, 89:145301, 2002.
  - [16] M. Kobayashi and M. Tsubota. Kolmogorov spectrum of superfluid turbulence: Numerical analysis of the gross-pitaevskii equation with a small-scale dissipation. *Phys Rev Lett*, 94:065302, 2005.
  - [17] M. La Mantia, D. Duda, M. Rotter, and L. Skrbek. Lagrangian accelerations of particles in superfluid turbulence. *Journal of Fluid Mechanics*, 717:R9, 2013.
  - [18] M. La Mantia. Particle dynamics in wall-bounded thermal counterflow of superfluid helium. *Phys Fluids*, 29:065102, 2017.
  - [19] W. F. Vinen. Mutual friction in a heat current in liquid helium ii. i. experiments on steady heat currents. *Proc. R. Soc. London A*, 240:114, 1957.
  - [20] C. F. Barenghi, Y. Sergeev, and A. Baggaley. Regimes of turbulence without an energy cascade. *Sci Rep*, 6:35701, 2017.
  - [21] T. Zhang and S. W. Van Sciver. Large-scale turbulent flow around a cylinder in counterflow superfluid4he (he (ii)). *Nat. Phys*, 1:36, 2005.
  - [22] G. P. Bewley, D. P. Lathrop, and K. P. Sreenivasan. Visualization of quantized vortices. *Nature*, 441:588, 2006.
  - [23] M. La Mantia, T. V. Chagovets, M. Rotter, and L. Skrbek. Testing the performance of a cryogenic visualization system on thermal counterflow by using hydrogen and deuterium solid tracers. *Rev Sci Instr*, 83:055109, 2012.
  - [24] W. Guo, S. B. Cahn, J. A. Nikkel, W. F. Vinen, and D. N. McKinsey. Visualization study of counterflow in superfluid helium-4 using metastable helium molecules. *Phys Rev Lett*, 105:045301, 2010.
  - [25] R. Hänninen and AW Baggaley. Vortex filament method as a tool for computational visualization of quantum turbulence. *Proc Natl Acad Sci USA*, page 201312535, 2014.
  - [26] L Galantucci, M Sciacca, and CF Barenghi. Coupled normal fluid and superfluid profiles of turbulent helium ii in channels. *Phys Rev B*, 92:174530, 2015.
  - [27] L Galantucci, M Sciacca, and CF Barenghi. Large-scale normal fluid circulation in helium superflows. *Phys Rev B*, 95:014509, 2017.
  - [28] Satoshi Yui, Makoto Tsubota, and Hiromichi Kobayashi. Three-dimensional coupled dynamics of the two-fluid model in superfluid he 4: Deformed velocity profile of normal fluid in thermal counterflow. *Physical review letters*, 120(15):155301, 2018.
  - [29] D Kivotides, CF Barenghi, and DC Samuels. Triple vortex ring structure in superfluid helium ii. *Science*, 290:777, 2000.
  - [30] O.C. Idowu, A. Willis, C. F. Barenghi, and D. C. Samuels. Local normal-fluid helium ii flow due to mutual friction interaction with the superfluid. *Phys Rev B*, 62:3409, 2000.

- [31] D Kivotides. Decay of finite temperature superfluid helium-4 turbulence. *J Low Temp Phys*, 181:68, 2015.
- [32] D Kivotides. Superfluid helium-4 hydrodynamics with discrete topological defects. *Phys Rev F*, 3:104701, 2018.
- [33] P. Gualtieri, F. Picano, G. Sardina, and C. M. Casciola. Exact regularized point particle method for multiphase flows in the two-way coupling regime. *Journal of Fluid Mechanics*, 773:520–561, 2015.
- [34] P. Gualtieri, F. Battista, and C. M. Casciola. Turbulence modulation in heavy-loaded suspensions of tiny particles. *Phys. Rev. Fluids*, 2:034304, Mar 2017.
- [35] D Kivotides. Spreading of superfluid vorticity clouds in normal-fluid turbulence. *J Fluid Mech*, 668:58, 2011.
- [36] F. London. *Superfluids*, volume 2. Wiley, New York, 1954.
- [37] R. J. Donnelly. *Quantized Vortices in Helium II*. Cambridge University Press, 1991.
- [38] S. K. Nemirovskii. Quantum turbulence: Theoretical and numerical problems. *Physics Report*, 524:85, 2013.
- [39] H.E. Hall and W.F. Vinen. The rotation of liquid helium ii. i. experiments on the propagation of second sound in uniformly rotating helium ii. *Proc. R. Soc. London A*, 238(1213):204, 1956.
- [40] H.E. Hall and W.F. Vinen. The rotation of liquid helium ii. ii. the theory of mutual friction in uniformly rotating helium ii. *Proc. R. Soc. London A*, 238(1213):215, 1956.
- [41] P Švančara and M La Mantia. Flight-crash events in superfluid turbulence. *Journal of Fluid Mechanics*, 876, 2019.
- [42] Brian Mastracci, Shiran Bao, Wei Guo, and William Frank Vinen. Particle tracking velocimetry applied to thermal counterflow in superfluid he 4: Motion of the normal fluid at small heat fluxes. *Physical Review Fluids*, 4(8):083305, 2019.
- [43] R. K. Childers and J. T. Tough. Helium ii thermal counterflow: Temperature- and pressure- difference data and analysis in terms of the vinen theory. *Phys Rev B*, 13:1040, 1976.
- [44] I. L. Bekarevich and I. M. Khalatnikov. Phenomenological derivation of the equations of vortex motion in he ii. *Sov. Phys JETP*, 13:643, 1961.
- [45] Russell J Donnelly. *Experimental superfluidity*. University of Chicago Press, 1967.
- [46] R. N. Hills and P. H. Roberts. Superfluid mechanics for a high density of vortex lines. *Arch. Rat. Mech. Anal.*, 66:43, 1977.
- [47] K. W. Schwarz. Turbulence in superfluid helium: steady homogenous counterflow. *Phys Rev B*, 18(1):245, 1978.
- [48] KW Schwarz. Three-dimensional vortex dynamics in superfluid he 4: Line-line and line-boundary interactions. *Phys Rev B*, 31(9):5782, 1985.
- [49] KW Schwarz. Three-dimensional vortex dynamics in superfluid he4. *Phys Rev B*, 38(4):2398, 1988.
- [50] H Adachi, S Fujiyama, and M Tsubota. Steady-state counterflow quantum turbulence: Simulation of vortex filaments using the full biot-savart law. *Phys Rev B*, 81:104511, 2010.
- [51] A. W. Baggaley, L. K. Sherwin, C. F. Barenghi, and Y. A. Sergeev. Thermally and mechanically driven quantum turbulence in helium ii. *Phys Rev B*, 86:104501, 2012.
- [52] L. K. Sherwin-Robson, C. F. Barenghi, and A. W. Baggaley. Local and nonlocal dynamics in superfluid turbulence. *Phys Rev B*, 91:104517, 2015.
- [53] RGKM. Aarts and ATAM de Waele. Numerical investigation of the flow properties of he ii. *Phys Rev B*, 50(14):10069, 1994.
- [54] A. W. Baggaley and S. Laizet. Vortex line density in counterflowing he ii with laminar and turbulent normal fluid velocity profiles. *Phys Fluids*, 25:115101, 2013.
- [55] D. Khomenko, L. Kondaurova, V.S. L’vov, P. Mishra, A. Pomyalov, and I. Procaccia. Dynamics of the density of quantized vortex-lines in superfluid turbulence. *Phys Rev B*, 91:180504(R), 2015.
- [56] A. W. Baggaley and J. Laurie. Thermal counterflow in a periodic channel with solid boundaries. *J Low Temp Phys*, 178:35–52, 2015.
- [57] S. Yui and M. Tsubota. Counterflow quantum turbulence of he-ii una square channel: Numerical analysis with nonuniform flows of the normal fluid. *Phys Rev B*, 91:184504, 2015.
- [58] D. C. Samuels. Response of superfluid vortex filaments to concentrated normal-fluid vorticity. *Phys Rev B*, 47(2):1107, 1993.
- [59] C.F. Barenghi, D.C. Samuels, G. Bauer, and R. J. Donnelly. Superfluid vortex lines in a model turbulent flow. *Phys Fluids*, 9:2631, 1997.
- [60] D Kivotides. Coherent structure formation in turbulent thermal superfluids. *Phys Rev Lett*, 96:175301, 2006.
- [61] K Morris, J Koplik, and DWI Rouson. Vortex locking in direct numerical simulations of quantum turbulence. *Phys Rev Lett*, 101:015301, 2008.
- [62] OC Idowu, D Kivotides, CF Barenghi, and DC Samuels. Equation for self-consistent superfluid vortex line dynamics. *J Low Temp Phys*, 120:269, 2000.
- [63] D Kivotides. Turbulence without inertia in thermally excited superfluids. *Phys Lett A*, 341:193, 2005.
- [64] D Kivotides. Relaxation of superfluid vortex bundles via energy transfer to the normal fluid. *Phys Rev B*, 76:054503, 2007.
- [65] D Kivotides. Energy spectra of finite temperature superfluid helium-4 turbulence. *Phys Fluids*, 26:105105, 2014.
- [66] D Kivotides. Interactions between normal-fluid and superfluid vortex rings in helium-4. *EPL*, 112:36005, 2015.
- [67] Saul Kaplun and PA Lagerstrom. Asymptotic expansions of navier-stokes solutions for small reynolds numbers. *Journal of Mathematics and Mechanics*, pages 585–593, 1957.
- [68] Saul Kaplun. Low reynolds number flow past a circular cylinder. *Journal of Mathematics and Mechanics*, pages 595–603, 1957.
- [69] Ian Proudman and JRA Pearson. Expansions at small reynolds numbers for the flow past a sphere and a circular cylinder. *Journal of Fluid Mechanics*, 2(3):237–262, 1957.
- [70] Milton Van Dyke. *Perturbation methods in fluid mechanics*. Parabolic Press, Stanford, Calif., annotated ed.. edition, 1975.
- [71] GE Volovik. Three nondissipative forces on a moving vortex line in superfluids and superconductors. *JETP LETTERS*

*C/C OF PIS'MA V ZHURNAL EKSPERIMENTAL'NOI TEORETICHESKOI FIZIKI*, 62:65–65, 1995.

- [72] L. Thompson and P. C. E. Stamp. Quantum dynamics of a bose superfluid vortex. *Phys. Rev. Lett.*, 108:184501, May 2012.
- [73] Russell J. Donnelly and Carlo F. Barenghi. The observed properties of liquid helium at the saturated vapor pressure. *J. Phys. Chem. Ref. Data*, 27(6):1217–1274, November 1998.
- [74] Uriel Frisch. *Turbulence: The Legacy of A. N. Kolmogorov*. Cambridge University Press, 1995.
- [75] A. W. Baggaley and C. F. Barenghi. Spectrum of turbulent kelvin-waves cascade in superfluid helium. *Phys Rev B*, 83:134509, 2011.
- [76] L Gamet, F Ducros, Franck Nicoud, and Thierry Poinsot. Compact finite difference schemes on non-uniform meshes. application to direct numerical simulations of compressible flows. *Int J Num Meth Fluids*, 29(2):159–191, 1999.
- [77] A. W. Baggaley and C. F. Barenghi. Tree method for quantum vortex dynamics. *J Low Temp Phys*, 166:3, 2012.
- [78] PG Saffman. *Vortex dynamics*. Cambridge University Press, 1992.
- [79] GP Bewley, MS Paoletti, KR Sreenivasan, and DP Lathrop. Characterization of reconnecting vortices in superfluid helium. *Proc Natl Acad Sci USA*, 105:13707, 2008.
- [80] S Serafini, L Galantucci, E Iseni, T Bienaime, R Bisset, CF Barenghi, F Dalfovo, G Lamporesi, and G Ferrari. Vortex reconnections and rebounds in trapped atomic bose-einstein condensates. *Phys Rev X*, 7:021031, 2017.
- [81] J Koplik and H Levine. Vortex reconnection in superfluid helium. *Phys Rev Lett*, 71:1375, 1993.
- [82] R Tebbs, A J. Youd, and CF Barenghi. The approach to vortex reconnection. *J Low Temp Phys*, 162(3-4):314, 2011.
- [83] RM Kerr. Vortex stretching as a mechanism for quantum kinetic energy decay. *Phys Rev Lett*, 106(22):224501, 2011.
- [84] M Kursu, K Bajer, and T Lipniaki. Cascade of vortex loops initiated by a single reconnection of quantum vortices. *Phys Rev B*, 83:014515, 2011.
- [85] A Villois, D Proment, and G Krstulovic. Universal and nonuniversal aspects of vortex reconnections in superfluids. *Phys Rev Fluids*, 2(4):044701, 2017.
- [86] L Galantucci, M Sciacca, and D Jou. The two fluid extended model of superfluid helium. *Atti Accad. Pelorit. Pericol. Cl. Sci. Fis. Mat. Nat.*, 97:A4, 2019.
- [87] RP Feynmann. *Application of quantum mechanics to liquid helium*, volume 1, chapter II, page 36. N Holland Publ Co, 1955.
- [88] AW Baggaley. The sensitivity of the vortex filament method to different reconnection models. *J Low Temp Phys*, 168(1-2):18–30, 2012.
- [89] M. van Hinsberg, J. Thije Boonkamp, F. Toschi, and H. Clercx. On the efficiency and accuracy of interpolation methods for spectral codes. *SIAM J. Sci. Comput.*, 34(4):B479–B498, January 2012.